ELSEVIER

Preparation of separative-phase fancy glaze derived from iron ore slag

Jianfeng Zhu, Pei Shi*, Fen Wang, Ting Zhao, Hao Jiang

School of Materials Science and Engineering, Shaanxi University of Science & Technology, Xi'an 710021, PR China

Abstract

The separative-phase fancy glaze was successfully prepared by using the iron ore residue as the ceramic colorant. A possible coloring mechanism was proposed to explain the variation of glaze colors and patterns with the increasing of firing temperature. Effects of the firing temperature on the chromaticity, precipitated phase and microstructure of separative-phase fancy glaze were investigated. The results indicated that with increasing the firing temperature, the content of whitlockite decreased while the size of phase separation droplets in glazes increased. The residual whitlockite weakened coloring of Fe_2O_3 and formed glaze patterns. In addition, the increased size of phase separation droplets weakened the structural color, which increased the $L*$ and $b*$ value of glazes. Therefore, the color of separative-phase fancy glaze got more yellow and brown gradually.
© 2015 Elsevier Ltd and Techna Group S.r.l. All rights reserved.

1. Introduction

With the rapid development of iron metallurgical industry, it has caused a huge amount of iron ore slag. Dumping or disposal of such great quantities of tailing occupies a large amount of land and causes damage to the ecological environment, which has determined that iron ore slag should look for technological development to ensure their viability in the short and long term. The iron ore slag contains iron, silica, alumina, calcium oxide etc., indicating that it is a valuable resource for recycling and utilizing [1–5].

During the past two decades, an increasing interest has been developed to explore the possible utilization of iron ore slag. Apart from recovering the valuable metals, the iron ore slag has been used to make the products like ceramic tiles, concrete, cement, glass-ceramics, waterproof mortar and pigment, confirming the possibilities of reusing such wastes to bring potential economic benefits and resolving the environmental problems [2–5]. Another great potential recycling method is to convert the wastes into ceramic glaze colorants.

Many types of industrial wastes, such as Al-rich anodizing sludge, Cr/Ni galvanizing sludge, foundry sand, ferrochromium fly ash and agricultural wastes, have been studied as ceramic glaze colorants, while the utilization of iron ore slag for ceramic glaze colorants has not been well considered [6–12]. Limited works have reported that reddish, black and blue glazes could be prepared by using the iron ore slag as colorants [1,13]. However, impurities in the wastes can affect the color of glazes as well as the decorative quality of products, which limit its applications and further commercial success. Fortunately, these problems could be solved by using iron ore slag as the separative-phase glaze colorant. According to the researches from Kingery and Wang et al. [14,15], the separative-phase glaze is an artistic glaze, in which decorative design can be formed by the color contrast of different phases due to its phase separation structures. This glaze has abundant colors and assortment styles, and is not high to the requirement of colorant. Therefore, the separative-phase glaze can be widely used in art porcelain, household porcelain, and building porcelain, etc. with substituting iron ore slag for the costly metallic oxides and pigments.

In this paper, to overcome the shortcomings of the conventional technologies, we attempted to utilize iron ore slag as the ceramic glaze colorant to prepare the phase separation fancy

*Corresponding author. Tel.: +86 2986131687; fax: +86 2986168188.
E-mail addresses: zhujf@sust.edu.cn (J. Zhu),
shipei7121@163.com (P. Shi).

Table 1
Chemical compositions of the iron ore slag (wt%).

SiO₂	Al₂O₃	Fe₂O₃	CaO	MgO	K₂O	TiO₂	P₂O₅	SO₃	MnO
26.37	11.61	41.54	5.96	0.40	6.10	6.02	0.37	0.66	0.29
BaO	Co₂O₃	ZrO₂	ZnO	CuO	SrO	Cr₂O₃	Y₂O₃	NiO	Rb₂O
0.20	0.11	0.09	0.07	0.06	0.05	0.04	0.02	0.02	0.02

glaze in the R_2O–RO–Al_2O_3–SiO_2–P_2O_5 basis system. The crystal phase composition and microstructure, the coloring mechanism and the physical property of the phase separation fancy glaze were investigated. This work will throw some light on the understanding of preparing phase separation fancy glaze by iron ore slag.

2. Experimental procedure

2.1. Materials

The iron ore slag was obtained from ShannXi Iron Group (China). To solve the problem of difficulty in grinding, this slag had already been ground into particles and passed through an 80 ASTM mesh sieve after magnetic separation process. The chemical and phase compositions of the waste were evaluated by X-ray fluorescence (XRF) and X-ray diffraction (XRD) analyses, respectively. Table 1 shows the chemical compositions of the investigated iron ore slag. It could be seen that in addition to the main components of Fe_2O_3, SiO_2, Al_2O_3, TiO_2, CaO and K_2O, a small amount of other oxides such as P_2O_5 and MgO were detected, which played an important role in the preparation of phase separation glazes. Additionally, cyanides, arsenic, lead and antimony were not presence in the iron ore residue except for 0.66 wt% sulfides. Because the content of sulfides is within the Comprehensive Emission Standard Limits of Air Pollutants (GB16297-1996, < 0.5 mg/m³) of China, SO_2 produced by decomposition of sulfides had little effect on the environment. Therefore, the use of industrial wastes as secondary raw materials was a very interesting Eco-purpose. Fig. 1 shows the XRD spectrum of iron ore slag. It was found that for this slag, the main crystalline phase includes hematite (Fe_2O_3), quartz (SiO_2) and anatase (TiO_2), all of which were the typical compositions of the slag after the iron ore processing.

2.2. Glaze preparation

The base glaze compositions were made by 60.6 wt% feldspar, 20.2 wt% quartz sand, 15.2 wt% calcite, 2 wt% talc and 2 wt% commercial grade calcium phosphate ($Ca_3(PO_4)_2$). Meanwhile 25 wt% iron ore slag was added as the colorant. Chemical compositions of the raw materials are also given in Table 2.

After weighing with 70 wt% water, 0.5 wt% sodium carboxyl methyl cellulose (CMC) and 0.2 wt% sodium tripolyphosphate (STP), the starting materials were directly milled at a rate of 300 r/min for 35 min to form the raw glaze slurry. Then the glaze slip was sieved and the density was adjusted to
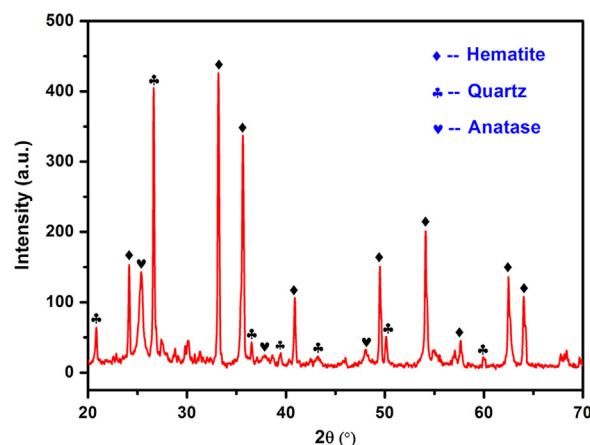

Fig. 1. The XRD patterns of the iron ore residue.

Table 2
Chemical compositions of the raw materials (wt%).

Raw materials	SiO₂	Al₂O₃	Fe₂O₃	CaO	MgO	K₂O	Na₂O	TiO₂	P₂O₅
Feldspar	69.94	17.41	0.51	3.54	1.01	0.51	7.08	–	–
Quartz	98.37	1.41	0.22	–	–	–	–	–	–
Calcite	0.67	–	–	98.68	0.65	–	–	–	–
Talc	64.64	–	0.06	0.24	34.96	0.06	0.04	–	–

1.5 g/cm³ by water. Subsequently, the glaze slip was applied to the biscuits test piece (Ø 4–5 cm) by dipping. After that, the test pieces were dried and fired at a heating rate of 3 °C/min to 900 °C and 1.5 °C/min to 1160 °C, 1190 °C, 1220 °C, 1250 °C, 1280 °C and 1310 °C, respectively, and then holding for 45 min at this temperature. Finally, the samples were cooled down to room temperature naturally in the furnace.

2.3. Characterization techniques

The chemical composition of the iron ore residue was determined by X-ray fluorescence (XRF-1800). The phase composition of the iron ore residue and phase separation fancy glazes were confirmed by X-ray diffraction (XRD) studies (D/max 2200 PC, Japan) using Cu K_α radiation ($\lambda = 1.5406$ Å) and scanning from $10°$ to $70°$ under 40 kV and 100 mA. The scanning rate was $8°$/min. And the color parameters ($L*$, $a*$, $b*$) of the fired specimens were measured by WSD-3C colorimeter using CIE Standard Illuminant D_{65}, following the CIE-$L*a*b*$ colorimetric method recommended by the CIE. On this method, $L*$ is the lightness axis (black (0)-white (100)), $a*$ is the green ($-$)-red ($+$) axis, and $b*$ is the blue ($-$)-yellow ($+$) axis. The bonding structure of the samples was studied by a Spectrum One FT-IR spectrometer (VERTE70) using KBr as the standard pellet in the range from 400 to 1800 cm^{-1}. The microstructure of the samples was investigated by scanning electron microscopy (SEM, HITACH, FE-S4800, Japan) equipped with an energy dispersive spectrometry (EDS). Before the testing, the surfaces of the samples were etched using 10 vol% HF for 30 s to expose
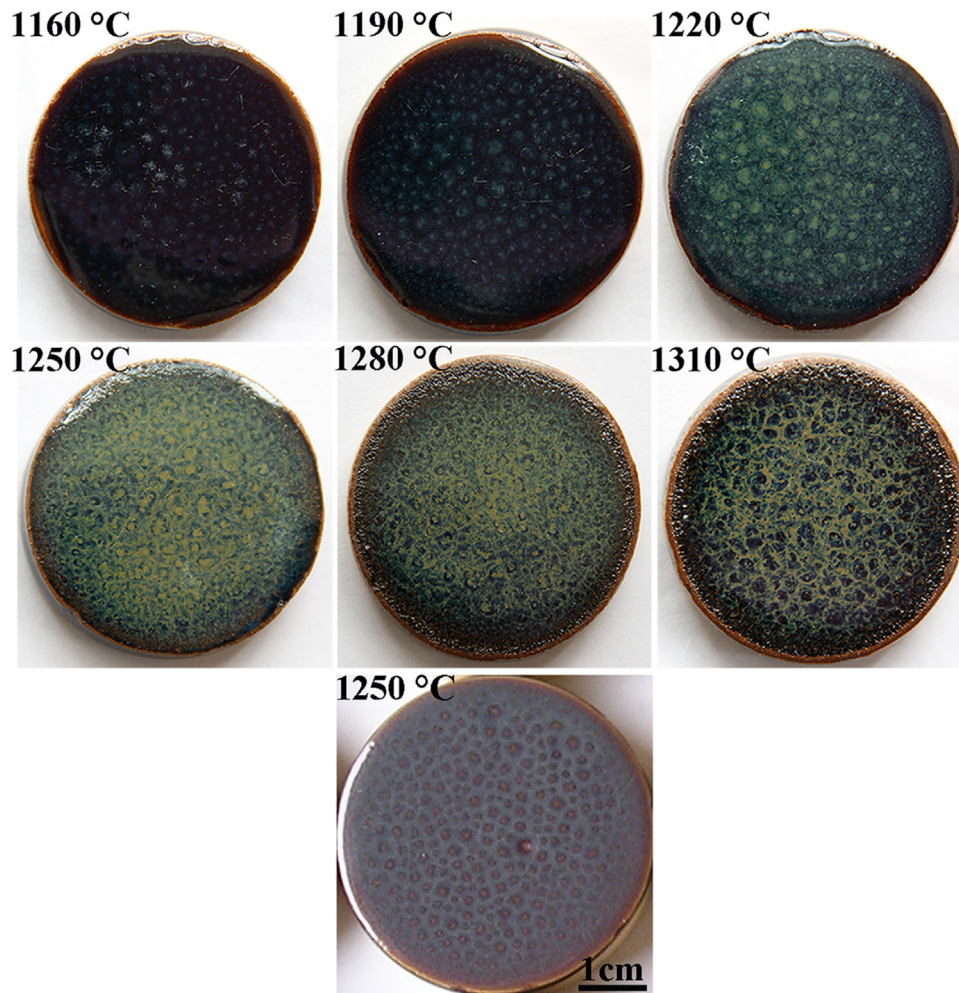
Fig. 2. Appearance of glazes with the iron ore residue in function of the firing temperature and glaze with the Fe_2O_3.

the crystal and phase separation structures. The mechanical properties of samples were evaluated after polishing their surfaces. Vickers hardness measurements were conducted on the HXD-1000 tester with a diamond indenter under a load of 50 N for 15 min. The wear resistance was measured by material surface performance tester (CFT-I) at the speed of 500 t/m (t and m denote the ton and meter respectively), with a load of 100 N for 20 min.

3. Results and discussion

Fig. 2 shows the appearance of the typical glazes with the iron ore residue and Fe_2O_3 as the ceramic colorant, respectively. It can be seen that, the glazes with the iron ore residue had more abundant colors and fancy than the glaze with the Fe_2O_3. So the iron ore residue was suit for the ceramic colorant of the separative-phase fancy glazes. Furthermore, the phenomenon of the dry glaze occurred at the edge of glazes when the firing temperature was higher than 1280 °C. The color values ($a*$, $b*$) and lightness ($L*$) parameters (whiteness) are listed in Table 3. For comparison, the $L*$ values first increased and then decreased with the increase of firing temperature, and presented local maxima at 1250 °C. In addition, negative values of $a*$ and $b*$

Table 3
$L*$, $a*$ and $b*$ values and glaze colors according to different temperatures.

Firing temperature (°C)	$a*$	$b*$	$L*$	Color
1160	−0.45	−3.08	15.45	Dark-blue
1190	−2.68	−5.69	16.83	Sea-blue
1220	−6.13	0.37	26.27	Green–blue
1250	−3.98	8.91	33.43	Yellow–green
1280	−3.94	6.33	32.32	Yellow–brown
1310	−3.09	5.98	29.48	Yellow–brown

were measured from the glazes at 1160–1190 °C, indicating that the values lay in the lower left quadrant (green and blue region) with coordinates. While fired the glazes at 1220–1310 °C, negative values of $a*$ and positive values of $b*$ were obtained, which indicated that the values lay in the under left quadrant (green and yellow region) with coordinates. Hence, it was found that the firing temperature was a main factor of the $L*$ and $b*$ values in the present system. Combining the performance and color of glaze surfaces at different firing temperatures, the glazes with better surface appearance and colors could be obtained at temperatures between 1190 and 1250 °C, and the glazes fired at 1160 °C, 1220 °C and 1280 °C need to be further researched.

Since the crystallization behavior of samples was greatly influenced by the firing temperature, it was necessary to clarify the formation of various crystalline phases created in separative-phase fancy glazes at the different firing temperatures, which could influence the physical properties of glazes. Fig. 3 shows the XRD patterns of the glazes fired at 1160 °C, 1220 °C and 1280 °C, respectively. The characteristic amorphous hump could be seen within the $2\theta \approx 15-35°$ range in all samples, which were associated to a large amount of aluminosilicate glass [16]. Meanwhile, some weak peaks, corresponding to whitlockite ($Ca_3(PO_4)_2$, PDF09-0169), quartz (SiO_2, PDF47-1144) and loveringite ($CaTi_{21}O_{38}$, PDF42-1368) crystallization, were observed when the firing temperatures were 1160 °C and 1220 °C. Among them, the whitlockite and quartz were probably from the starting composition, while
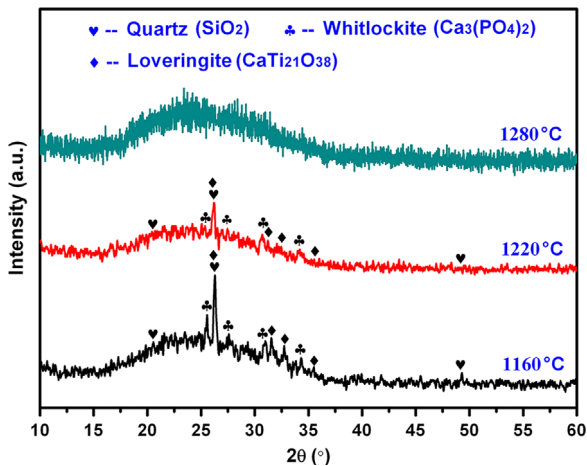
the loveringite was probably crystallized from the reaction of CaO and TiO_2. With increasing the firing temperature, the intensity of the crystallization peaks decreased until the main phase became glass at 1280 °C. Due to the very few content of loveringite in glazes, it had little influence on the opacity and strength of the glaze surfaces. As a result, the presence of withlockite and quartz were only considered.

Fig. 4 shows the STEM/EDS elemental analysis of the etched glazes surface at different firing temperatures. Due to the acid treatment, some aggregate crystals were observed on the glaze surface at 1160 °C, while they diffused at 1220 °C and finally disappeared at 1280 °C. Moreover, strong Ca and P signals were detected from the aggregate crystals, indicating that these crystals might be whitlockite rather than quartz.

Fig. 5 displays the enlarged images and EDS analysis, measured on the microspots denoted by the numbers 1–2 (Fig. 4). It could be clearly seen that a large number of irregular shaped crystals disorderly distributed in glass matrix. The chemical compositions of crystals was analyzed by EDS in Fig. 5, measured on the microspots denoted by the position 1 and 2 in the SEM images. It showed that the crystals in position 1 and 2 were all rich in Ca, P and O. Combining with the XRD analysis in Fig. 3, they were inferred as the residue whitlockite which formed big aggregates (Fig. 4). The results further indicated that the glaze surfaces formed patterns, which was due to the crystallization of whitlockite at 1160 °C and 1220 °C. When these crystals existed in the glaze surfaces, they could weaken the coloring performance of Fe_2O_3 and formed glaze patterns. Furthermore, the color of patterns was lighter than that of the glazes. Additionally, when the whitlockite melted entirely, the content of Fe_2O_3 in crystals decreased. More Fe^{2+} was oxidized to Fe^{3+} at 1280 °C, so the yellow patterns appeared on the glaze surface [17].

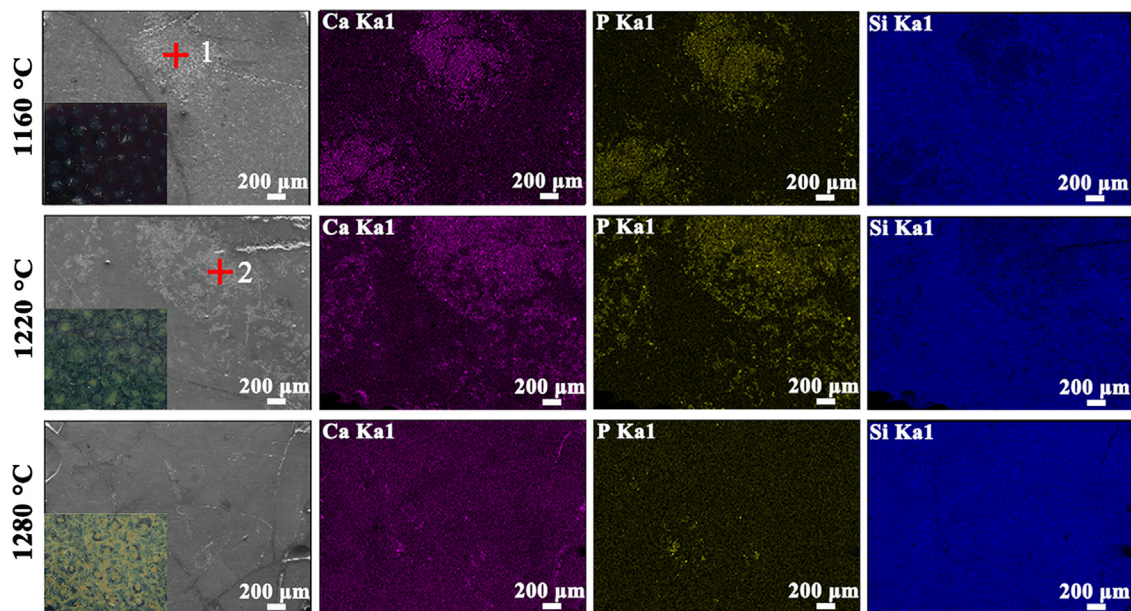Fig. 3. The XRD patterns of separative-phase fancy glazes with different firing temperatures.

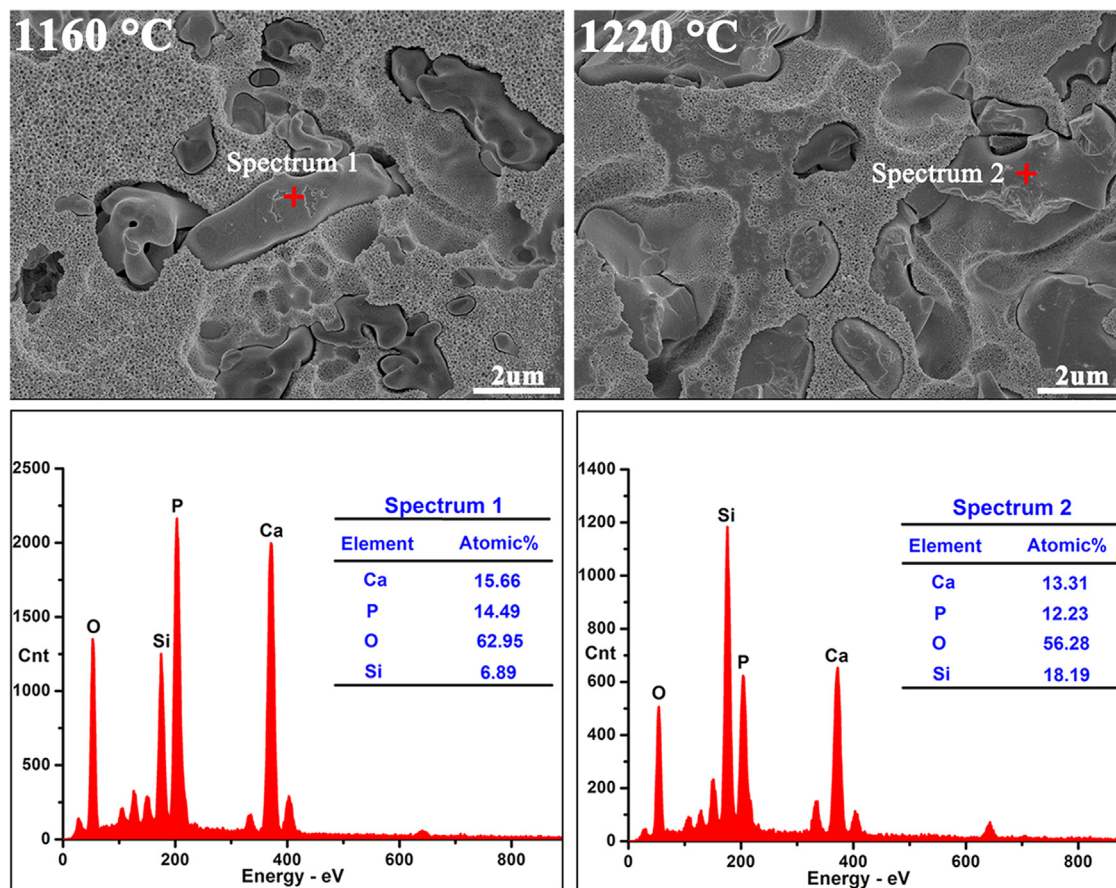Fig. 4. The SEM images and elemental mapping images of Ca K and P K edges for samples.

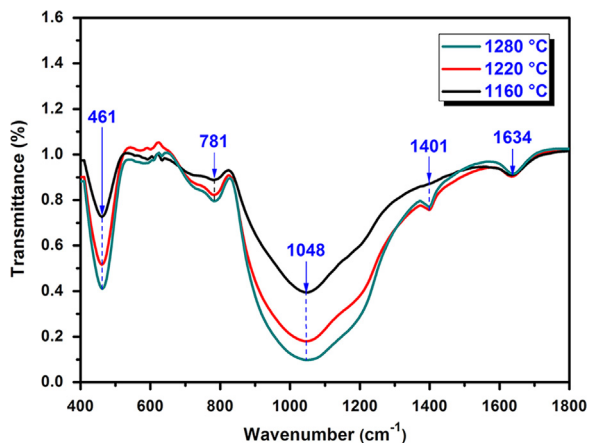Fig. 5. SEM images of crystals and EDS spectra on the glaze surfaces at 1160 °C and 1220 °C.

Fig. 6. FT-IR spectrum of the glazes with different firing temperatures.

The IR absorbance spectra of investigated glazes are illustrated in Fig. 6. All the spectra showed five characteristic peaks located at $1634\,cm^{-1}$, $1401\,cm^{-1}$, $1048\,cm^{-1}$, $781\,cm^{-1}$ and $461\,cm^{-1}$, respectively. The absorption band at $1634\,cm^{-1}$ was close to the position of H_2O bending vibrations. The smaller intensity bands at $1401\,cm^{-1}$ and $781\,cm^{-1}$, could be assigned to the $(PO_4)^{3-}$ asymmetric stretches of P–O–P bond. The absorption band at $1048\,cm^{-1}$ was assigned to the stretching vibration of Si–O, which indicated that the structure of the tested glazes was dominated by the so-called Q^3 group (where Q is the number of bridging oxygen) [18,19]. The band at $461\,cm^{-1}$ could be linked with the bending vibrations of two types of bridge bonds Si–O–Si and Si–O–Al [19]. Comparing decomposition of studied glazes the differences in the intensity of the bands associated with the stretching vibrations of Si–O and the bridging vibration of Si–O–Si and Si–O–Al were especially visible. Additionally, intensity of the $(PO_4)^{3-}$ asymmetric stretches of P–O–P bond also increased with a simultaneous increase of the band intensity. It could be concluded that the increasing firing temperature led to the break of $(SiO_4)^{4-}$ and $(PO_4)^{3-}$ tetrahedra in the separative-phase glazes, destroying the covalent amorphous network. As a result, the viscosity of molten glazes decreased with the increasing of firing temperature.

Fig. 7 presents the SEM micrographs of samples with different firing temperatures of 1160 °C, 1220 °C and 1280 °C. It could be shown that the discrete droplet phase separation structures were formed in every sample [20]. Additionally, with the increase of firing temperature, the average diameter of the phase separation droplets increased while the density decreased in the glazes, which were due to the decreased viscosity of the molten glazes at higher firing temperatures. Therefore, the movement speed of particles got faster so that the discrete phase droplet could easily move to the surface of phosphate glass [21].
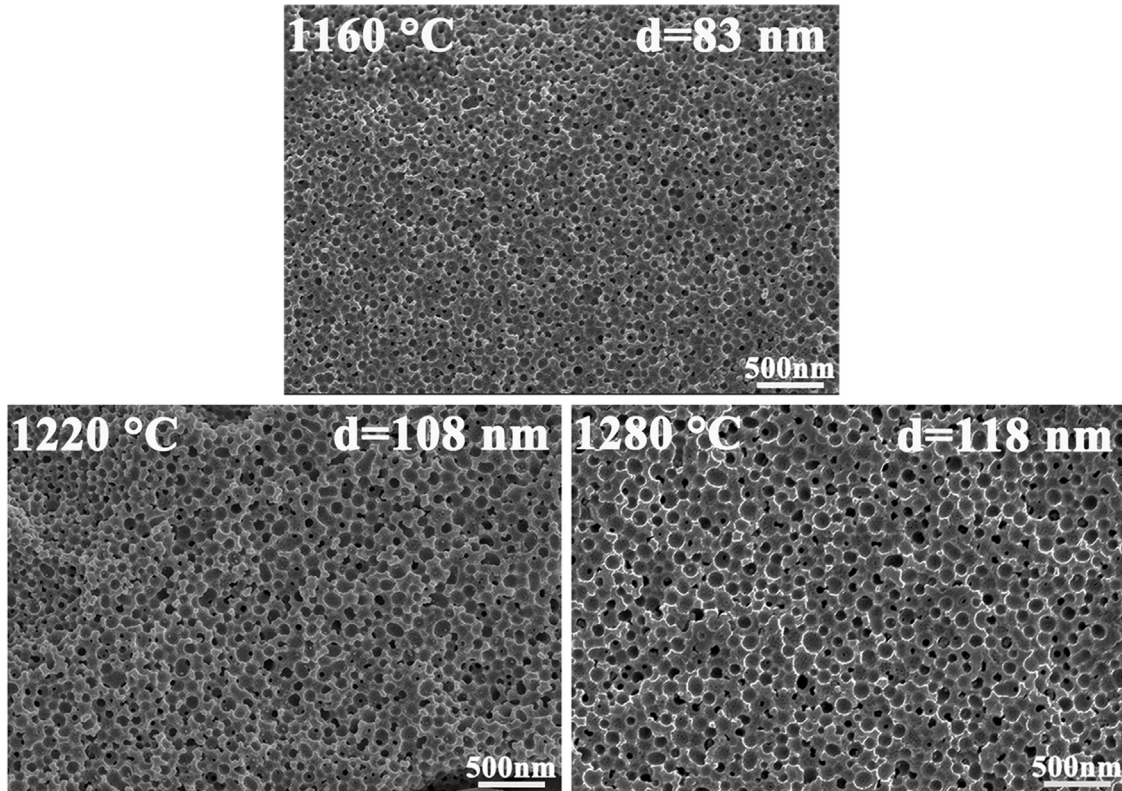
Fig. 7. Typical SEM images of separation structure on the sample surfaces at different firing temperatures.
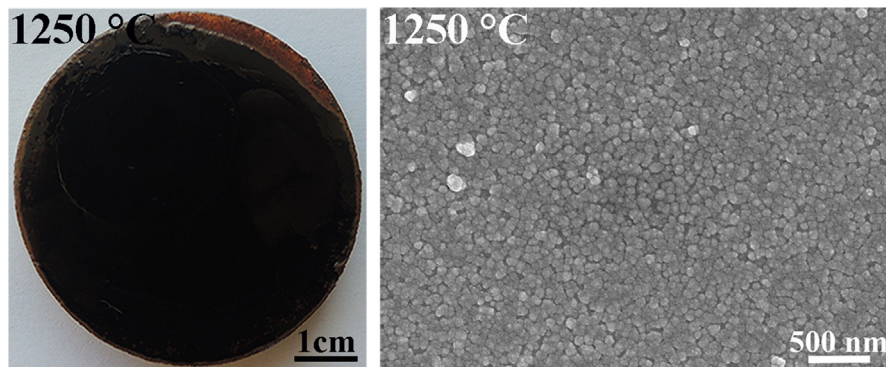

Fig. 8. Appearance and SEM micrograph of the glaze with addition of 25 wt% iron ore residue but without calcium phosphate at 1250 °C.

Due to a three-dimensional amorphous structure of the short-range order instead of the long-range order in the separative-phase glaze, it was the main source of the structural color. The structural color of the object was caused by optical effects developed by microstructure such as interference, diffraction and reflection when the size range of the object was comparable to the optical wavelength range [22,23]. The developing color strongly depended on the refractive index and the size of periodic structure [23]. Its color rending principle could be analyzed by the Rayleigh scattering. When the size of scattering particles was 1–300 nm, the Rayleigh scattering might occur in glaze. The scattering intensity was determined with the following formulas [15,24].

$$I(\lambda)_{\text{scattering}} \propto \frac{I(\lambda)_{\text{incident}}}{\lambda^4} \qquad (1)$$

where $I(\lambda)_{\text{incident}}$ and λ are intensity and wavelength of the incident light, respectively. The smaller the λ, the easier the Rayleigh scattering. Since blue light was at the short wavelength end of the visible spectrum, it was scattered in the atmosphere much more than the longer-wavelength red light. As a result, the structural color developed by the Rayleigh scattering showed that blue and the glaze colors became blue with addition of calcium phosphate [25]. In order to prove the Rayleigh
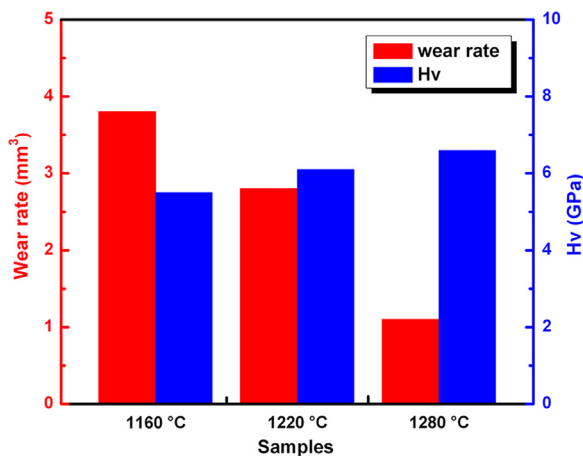
Fig. 9. The wear rate and Vickers hardness of separative-phase fancy glazes versus firing temperature.

scattering caused by calcium phosphate, the appearance and SEM micrograph of the glaze with addition of 25 wt% iron ore residue but without calcium phosphate are shown in Fig. 8. Apparently, the discrete droplet phase separation structures were not formed in the glaze, indicating that the Rayleigh scattering could not occur on the glaze surface. Hence, the glaze color was deep brown instead of blue. When the size of phase separation droplets became larger, the scattering intensity ($I(\lambda)_{incident}$) was smaller and the opalescence blue formed by structural color was lighter. So the blue of glaze surface was lighter with the increasing of firing temperature.

In order to evaluate the suitability of materials for series production in technologies, the properties of the produced samples fired at different temperatures were measured. And the abrasive resistance and hardness are summarized in Fig. 9. The results show that the wear rate gradually decreased from 3.80 to 1.09 mm^3 as the firing temperature increased from 1160 to 1280 °C. On the contrary, the Vickers hardness increased progressively with the increment of firing temperature. And the glaze fired at 1280 °C possessed the maximum hardness value of 6.6 GPa. Due to the lower mechanical properties of whitlockite than glass, the increase in wear resistance and hardness partially derived from the low whitlockite content at high temperatures (Fig. 3) [26]. However, the fault "dry glaze" of glaze surfaces appeared when the firing temperatures exceeded 1280 °C. The optimal comprehensive properties are obtained at 1250 °C, with the low value of wear rate (2.8 mm^3) and the high value of hardness (6.1 GPa), the good surface appearance and color, indicating that the separative-phase fancy glaze with desirable physical and mechanical properties could be successfully synthesized at this temperature. The separative-phase fancy glaze had attracted special industrial interest because of the good properties, the relatively simple conditions of firing and their wide use in many applications.

4. Conclusion

The separative-phase fancy glazes were produced with the addition of 25 wt% iron ore residue as the ceramic colorant instead of metallic oxides and pigments. The optimal firing temperature ranged from 1190 °C to 1250 °C were selected through analyzing the relationship between the firing temperature and quality of glaze surface appearance. According to the XRD and SEM results, with increasing the firing temperature, the content of whitlockite decreased, which weakened the coloring of Fe_2O_3 and formed glaze patterns. While the size of patterns gradually increased at 1160–1220 °C. Additionally, when the whitlockite melted entirely, the content of Fe_2O_3 in the crystals decreased so that patterns appeared on the glaze surface. The SEM microstructure showed that the discrete droplet phase separation structures were developed in glazes and their sizes were less than 300 nm, so the structural color was formed owing to the Rayleigh scattering and the glaze color got blue. A dual coloring changing mechanism with the increasing of the firing temperature was in effect for the separative-phase fancy glaze, covering the Fe_2O_3 content and the varying size of phase separation droplet. The chemical color of Fe_2O_3 was the main coloring factor, and the structural color formed by phase separation droplet acted as the auxiliary coloring in the glaze. Besides, the presence of whitlockite was the reason for forming patterns on the glaze surfaces at 1160 °C and 1220 °C.

References

[1] L.H. Zhao, Y. Li, Y.Y. Zhou, D.Q. Cang, Preparation of novel ceramics with high CaO content from steel slag, Mater. Des. 64 (2014) 608–613.

[2] Oscar Costa Pereira, Adriano Michael Bernardin, Ceramic colorant from untreated iron ore residue, J. Hazard. Mater. 233–234 (2012) 103–111.

[3] Z.H. Yang, Q. Lin, J.X. Xia, Y. He, G.D. Liao, Y. Ke, Preparation and crystallization of glass–ceramics derived from iron-rich copper slag, J. Alloy. Compd. 574 (2013) 354–360.

[4] S.J. Zhao, J.J. Fan, W. Sun, Utilization of iron ore tailings as fine aggregate in ultra-high performance concrete, Constr. Build. Mater. 50 (2014) 540–548.

[5] S.J. Liu, Q.Q. Hu, F.Q. Zhao, X.M. Chu, Utilization of steel slag, iron tailings and fly ash as aggregates to prepare a polymer-modified water-proof mortar with a core–shell styrene–acrylic copolymer as the modifier, Constr. Build. Mater. 72 (2014) 15–22.

[6] Enrico Inès Ponsot, Bernardo, Self glazed glass ceramic foams from metallurgical slag and recycled glass, J. Clean. Prod. 59 (2013) 245–250.

[7] L.M. Schabbach, G. Bolelli, F. Andreola, I. Lancellotti, L. Barbieri, Valorization of MSWI bottom ash through ceramic glazing process: a new technology, J. Clean. Prod. 23 (2012) 147–157.

[8] L.M. Schabbach, F. Andreola, L. Barbieri, I. Lancellotti, E. Karamanova, B. Ranguelov, A. Karamanov, Post-treated incinerator bottom ash as alternative raw material for ceramic manufacturing, J. Eur. Ceram. Soc. 32 (2012) 2843–2852.

[9] Fernanda Andreola, Luisa Barbieri, Federica Bondioli, Agricultural waste in the synthesis of coral ceramic pigment, Dyes Pigment. 94 (2012) 207–211.

[10] W. Hajjaji, G. Costa, C. Zanelli, M.J. Ribeiro, M.P. Seabra, M. Dondi, J. A. Labrincha, An overview of using solid wastes for pigment industry, J. Eur. Ceram. Soc. 32 (2012) 753–764.

[11] Mohammed A. Binhussain, Mauro Marangoni, Enrico Bernardo, Paolo Colombo, Sintered and glazed glass-ceramics from natural and waste raw materials, Ceram. Int. 40 (2014) 3543–3551.

[12] H.Z. Yang, C.P. Chen, L.J. Pan, H.X. Lu, H.W. Sun, X. Hu, Preparation of double-layer glass-ceramic/ceramic tile from bauxite tailings and red mud, J. Eur. Ceram. Soc. 29 (2009) 1887–1894.

[13] Y. Wang, Development of black fancy blue glaze using iron tailings, China Ceram. 49 (2013) 58–61.

[14] W.D. Kingery, P.B. Vandiver, I.W. Huang, Y.M. Chiang, Liquid–liquid immiscibility and phase separation in the quaternary systems $K_2O–Al_2O_3–CaO–SiO_2$ and $Na_2O–Al_2O_3–CaO–SiO_2$, J. Non-Cryst. Solids 54 (1983) 163–171.

[15] F. Wang, H.J. Luo, Q. Li, W.D. Li, Characteristic and coloring mechanism of the separative-phase colored ceramic, J. Chin. Ceram. Soc. 37 (2009) 181–186.

[16] X.S. Cheng, S.J. Ke, Q.H. Wang, H. Wang, A.Z. Shui, P.A. Liu, Characterization of transparent glaze for single-crystalline anorthite porcelain, Ceram. Int. 38 (2012) 4901–4908.

[17] W. David Kingery, Pamela B. Vandiver, Ceramic masterpieces: art, structure and technology, Free Press, New York, 1983.

[18] Ishu Kansal, Ashutosh Goel, Dilshat U. Tulyaganov, Raghu Raman Rajagopal, José M.F. Ferreira, Structural and thermal characterization of $CaO–MgO–SiO_2–P_2O_5–CaF_2$ glasses, J. Eur. Ceram. Soc. 32 (2012) 2739–2746.

[19] Janusz Partyka, Maciej Sitarz, Magdalena Leśniak, Katarzyna Gasek, Piotr Jeleń, The effect of SiO_2/Al_2O_3 ratio on the structure and microstructure of the glazes from $SiO_2–Al_2O_3–CaO–MgO–Na_2O–K_2O$ system, Spectrochim. Acta A 134 (2015) 621–630.

[20] Encarna Bou, Arnaldo Moreno, Agustín Escardino, Ana Gozalbo, Microstructural study of opaque glazes obtained from frits of the system: $SiO_2–Al_2O_3–B_2O_3–(P_2O_5)–CaO–K_2O–TiO_2$, J. Eur. Ceram. Soc. 22 (2007) 1791–1796.

[21] Francisco Jose Torres, Javier Alarcón, Pyroxene-based glass-ceramics as glazes for floor tiles, J. Eur. Ceram. Soc. 25 (2005) 349–355.

[22] Shuichi Kinoshita, Shinya Yoshioka, Structural colors in nature: the role of regularity and irregularity in the structure, ChemPhysChem 6 (2005) 1442–1459.

[23] Kenji Higashiguchi, Masafumi Inoue, Tomohiro Oda, Kenji Matsuda, Solvent-responsive structural colored balloons, Langmuir 28 (2012) 5432–5437.

[24] Ryan Thalman, Kyle J. Zarzana, Margaret A. Tolbert, Rainer Volkamer, Rayleigh scattering cross-section measurements of nitrogen, argon, oxygen and air, J. Quant. Spectrosc. Radiat. Transf. 147 (2014) 171–177.

[25] Y.M. Yang, M. Feng, X. Ling, Z.W. Mao, C.S. Wang, X.M. Sun, M. S. Guo, Microstructural analysis of the color-generating mechanism in Ru ware, modern copies and its differentiation with Jun ware, J. Archaeol. Sci. 32 (2005) 301–310.

[26] Ediz Ercenk, The crystallization kinetics of the $CaO–SiO_2–P_2O_5–MgO–Al_2O_3$ base glass system, J. Non-Cryst. Solids 387 (2014) 101–106.